Hidden Time Reversal in Driven *XXZ* Spin Chains: Exact Solutions and New Dissipative Phase Transitions

Mingxing Yao,[1,*] Andrew Lingenfelter,[1,2] Ron Belyansky,[1] David Roberts,[3] and Aashish A. Clerk[1,†]
[1]*Pritzker School of Molecular Engineering, University of Chicago, Chicago, Illinois 60637, USA*
[2]*Department of Physics, University of Chicago, Chicago, Illinois 60637, USA*
[3]*Joint Quantum Institute, NIST/University of Maryland, College Park, Maryland 20742, USA*

(Received 26 July 2024; revised 11 December 2024; accepted 6 March 2025; published 4 April 2025)

We show that several models of interacting *XXZ* spin chains subject to boundary driving and dissipation possess a subtle kind of time-reversal symmetry, making their steady states exactly solvable. We focus on a model with a coherent boundary drive, showing that it exhibits a unique continuous dissipative phase transition as a function of the boundary drive amplitude. This transition has no analog in the bulk closed system or in incoherently driven models. We also show the steady-state magnetization exhibits a surprising fractal dependence on interaction strength, something previously associated with less easily measured infinite-temperature transport quantities (the Drude weight). Our exact solution also directly yields driven-dissipative double-chain models that have pure, entangled steady states that are current carrying.

DOI: 10.1103/PhysRevLett.134.130404

Introduction—The nonequilibrium dynamics of driven interacting systems represents a forefront in quantum many-body physics. Among such systems, driven integrable spin chains are a paradigmatic class of models [1–3], studied for their broad relevance to experimental platforms [4–8], as well as for the deep theoretical insights enabled by the tools of quantum integrability. They exhibit many surprising phenomena, including unexpected connections to Kardar-Parisi-Zhang universality [9–12], transitions between ballistic, diffusive, and insulating transport regimes [13,14], and fractal structures in the Drude weight characterizing ballistic transport [15–17]. Models where boundary driving is balanced with boundary dissipation are also uniquely interesting: their nonequilibrium steady states (NESSs) exhibit a rich set of phenomena that reflect the physics of the bulk Hamiltonian. Remarkably, a number of such models (where the driving is incoherent) admit an analytic solution for the NESS [16,18–20].

Given this wide body of work, there are two natural questions that arise. First, is it possible to have phase transitions in the NESSs of boundary-driven-dissipative spin chains that are controlled by the boundary drive alone and that *do not* simply reflect different phases of the bulk Hamiltonian? While previous studies have seen transitions in either transport properties or correlation structure [21], they involve tuning a parameter in the bulk Hamiltonian, and are simply related to its structure. Second, is there a more general way to understand the remarkable exact solutions in Refs. [13,16,20,22]? If so, can we use this to derive qualitatively new exact solutions?

In this Letter, we address both these questions. We show that a version of quantum detailed balance [hidden time-reversal symmetry (hTRS) [23]] is present in a variety of boundary-driven-dissipative *XXZ* spin chain models, enabling exact analytic solutions of the NESSs via the coherent quantum absorber (CQA) construction [23,24] (see Fig. 1). This method provides a new, physically appealing way to understand previously derived exact solutions and lets us derive completely new solutions. hTRS has previously been used to describe many-body models with purely collective interactions [25–27] or boundary-driven models that are noninteracting in the bulk [28]; unlike those previous works, here we apply it to a truly interacting spin chain model. We use it to find an exact solution for the NESSs of a *XXZ* spin chain subject to boundary loss and a "coherent" boundary drive (see Fig. 1). Dissipative many-body systems with coherent boundary drives are relatively unstudied, but can have remarkable behavior [29,30]. Unlike previously studied *XXZ* models with incoherent drives, our NESS exhibits a continuous phase transition as a function of the boundary drive amplitude, a transition that has no simple correspondence to ground-state phases of the bulk *XXZ* Hamiltonian. The transition can be seen by measuring the average magnetization or spin current. We also find that the steady-state magnetization mirrors the surprising fractal structure of the infinite-temperature *XXZ* model Drude weight [15], an effect related to the

*Contact author: mxyao@uchicago.edu
†Contact author: aaclerk@uchicago.edu

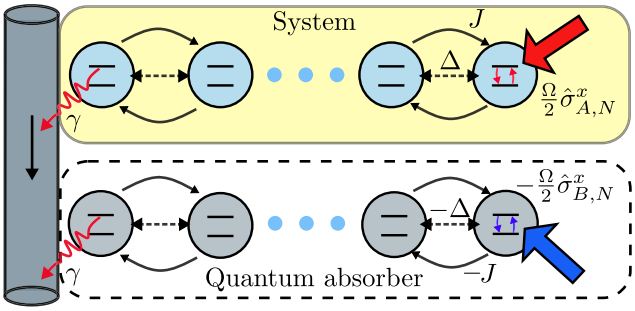

FIG. 1. Schematic of the boundary-driven XXZ spin chain and the CQA construction of the doubled system. The system (top) consists of N spins with a coherent drive at site N (right) and incoherent loss at site 1 (left). The absorber (bottom) consists of mirroring the system and is coupled to the system via a unidirectional waveguide.

quasiparticle structure of the bulk XXZ Hamiltonian. This represents perhaps the simplest observable manifestation of this effect.

Our Letter reveals other surprising structures. The connection to hTRS allows us to also construct exactly solvable models where two boundary-driven XXZ chains are coupled via common waveguide (see Fig. 1). These systems exhibit a pure, current-carrying steady state, with a steady-state entanglement that grows logarithmically with system size. Furthermore, the presence of hTRS in these driven-dissipative interacting spin models not only helps determine the steady state but also implies that certain steady-state correlation functions exhibit Onsager symmetry.

Model—We consider a driven-dissipative system of N spins $1/2$ governed by the Gorini-Kossakowski-Sudarshan-Lindblad (Lindblad) master equation

$$\partial_t\hat{\rho} = \hat{\mathcal{L}}\hat{\rho} = -i\left[\hat{H}_{XXZ} + \frac{\Omega}{2}\hat{\sigma}^x_N, \hat{\rho}\right] + \gamma\mathcal{D}[\hat{\sigma}^-_1]\hat{\rho}, \tag{1}$$

where $\hat{H}_{XXZ} = \sum_{j=1}^{N-1}(J\hat{\sigma}^x_j\hat{\sigma}^x_{j+1} + J\hat{\sigma}^y_j\hat{\sigma}^y_{j+1} + \Delta\hat{\sigma}^z_j\hat{\sigma}^z_{j+1})$ is the XXZ Hamiltonian, with $\hat{\sigma}^x, \hat{\sigma}^y, \hat{\sigma}^z$ being the Pauli matrices, Ω is the amplitude of the coherent drive on site N, and $\mathcal{D}[\hat{L}]\hat{\rho} \equiv \hat{L}\,\hat{\rho}\,\hat{L}^\dagger - \frac{1}{2}\{\hat{L}^\dagger\hat{L}, \hat{\rho}\}$ is the Lindblad dissipator, describing the boundary decay with jump operator $\hat{L} = \hat{\sigma}^-_1$ and rate γ. Equation (1) is naturally feasible in experimental platforms such as superconducting circuits and Rydberg atoms [29,31–33].

In this Letter, we focus on the NESS $\hat{\rho}_{\rm ss} \equiv \lim_{t\to\infty} e^{\hat{\mathcal{L}}t}\hat{\rho}(0)$ of this master equation, which, as shown in Supplemental Material [34], is unique for all parameters J, Δ, Ω, γ.

We find the steady state of Eq. (1) using the CQA method [23,24]. The basic idea is to redirect the dissipation of the system of interest ("A") to an absorber system ("B") via a chiral waveguide (see Fig. 1). The absorber is designed such that the combined $A+B$ system relaxes to a pure dark state $|\psi_{\rm CQA}\rangle$. The steady state of system A is obtained by tracing out the absorber $\hat{\rho}_{\rm ss} = {\rm Tr}_B(|\psi_{\rm CQA}\rangle\langle\psi_{\rm CQA}|)$. For a system with hTRS [23] (as we find to be the case here), there is a simple construction of the absorber system B: one mirrors the original spin chain with $\hat{H}^{(B)} = -\hat{H}^{(A)}$ and $\hat{L}^{(B)} = -\hat{L}^{(A)}$ (see Supplemental Material [34]). The dynamics of this doubled system $\hat{\rho}_{\rm AB}$ is described by the cascaded master equation $\partial_t\hat{\rho}_{\rm AB} = -i[\hat{H}^{(AB)}, \hat{\rho}] + \gamma\mathcal{D}[\hat{L}^{(AB)}]\hat{\rho}$ where

$$\hat{H}^{(AB)} = \hat{H}^{(A)}_{XXZ} - \hat{H}^{(B)}_{XXZ} + \frac{\Omega}{2}(\hat{\sigma}^x_{A,N} - \hat{\sigma}^x_{B,N}) + \hat{H}_c, \tag{2}$$

$$\hat{L}^{(AB)} = \hat{\sigma}^-_{A,1} - \hat{\sigma}^-_{B,1}, \tag{3}$$

and $\hat{H}_c = -(i\gamma/2)(\hat{\sigma}^+_{A,1}\hat{\sigma}^-_{B,1} - \hat{\sigma}^-_{A,1}\hat{\sigma}^+_{B,1})$ is the unidirectional coupling between the system and absorber [40,41], leading to effective isolation of system from absorber [42]. We search for a pure state satisfying the dark-state conditions $\hat{H}^{(AB)}|\psi_{\rm CQA}\rangle = 0$ and $\hat{L}^{(AB)}|\psi_{\rm CQA}\rangle = 0$.

We consider the doubled system to be a chain of N sites, but with a doubled local Hilbert space spanned by the four states: $|0_i\rangle \equiv |{\downarrow_{A,i}}{\downarrow_{B,i}}\rangle$, $|1_i\rangle \equiv |{\uparrow_{A,i}}{\uparrow_{B,i}}\rangle$, $|S_i\rangle \equiv (|{\uparrow_{A,i}}{\downarrow_{B,i}}\rangle - |{\downarrow_{A,i}}{\uparrow_{B,i}}\rangle)/\sqrt{2}$, and $|T_i\rangle \equiv (|{\uparrow_{A,i}}{\downarrow_{B,i}}\rangle + |{\downarrow_{A,i}}{\uparrow_{B,i}}\rangle)/\sqrt{2}$. Here $|\uparrow\rangle$, $|\downarrow\rangle$ denote $\hat{\sigma}_z$ eigenstates with eigenvalues ±1, respectively, and $\hat{\sigma}^- = |\downarrow\rangle\langle\uparrow|$. Inspired by the matrix product operator (MPO) ansatz of Ref. [16], we construct the pure (unnormalized) dark state as a matrix product state (MPS) ansatz

$$|\psi_{\rm CQA}\rangle = \sum_{s_1,\ldots,s_N} \mathbf{v}_{\mathbf{L}}^\dagger \hat{A}_{s_1}\ldots\hat{A}_{s_N}\mathbf{v}_{\mathbf{R}}|s_1\ldots s_N\rangle. \tag{4}$$

Here, the summation is limited to the triplet subspace $s_i \in \{0_i, 1_i, T_i\}$, as the singlet state $|S_i\rangle$ decouples due to the dark-state conditions (see Supplemental Material [34]). The matrices $\hat{A}_s$ are assumed translationally invariant and represented by the ansatz: $\hat{A}_T = \sum_{k=0}^{N} a_k|k\rangle\langle k|$, $\hat{A}_1 = \sum_{k=0}^{N-1} b_k|k+1\rangle\langle k|$, and $\hat{A}_0 = \sum_{k=0}^{N-1} c_k|k\rangle\langle k+1|$, where $\{|k\rangle, k = 0, 1, \ldots, N\}$ labels the auxiliary space (which we view as a one-dimensional lattice). The left vector $\mathbf{v}_{\mathbf{L}}$, corresponding to the dissipative site, is chosen to be $|0\rangle$ (i.e., the leftmost site in the auxiliary lattice), while the right vector $\mathbf{v}_{\mathbf{R}}$, corresponding to the coherently driven site, is parametrized as $\mathbf{v}_{\mathbf{R}} = \sum_{k=0}^{N}\alpha_k|k\rangle$. Imposing the dark-state condition on the state in Eq. (4) yields recursion relations for the matrix elements a_k, b_k, c_k and the coefficients α_k. These relations can be efficiently solved numerically exactly but also approximately analytically in certain limits (see Supplemental Material [34]). Note that $\hat{A}_s$ changes the auxiliary state by at most 1, which implies that the bond dimension of the MPS scales at most linearly with N.

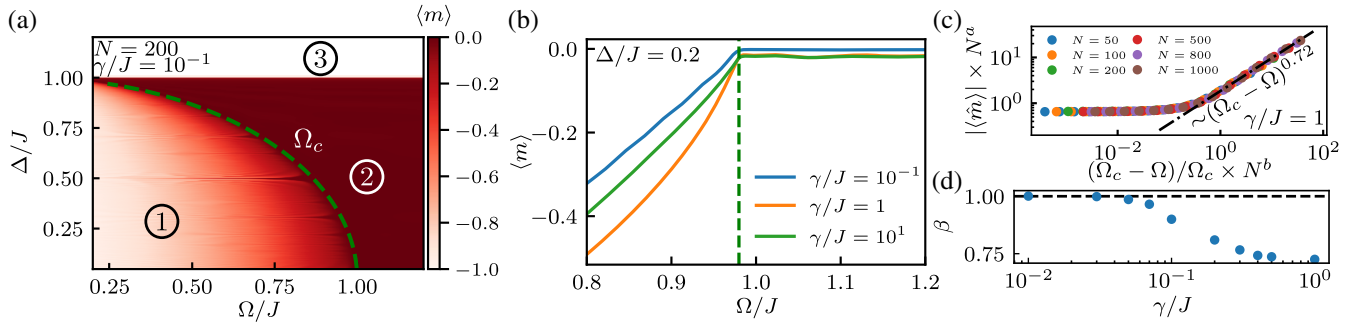

FIG. 2. Phase diagram. (a) Magnetization density $\langle m \rangle$ in the steady state as a function of Δ/J and Ω/J. The three phases are denoted by (1) the ballistic ordered phase, (2) ballistic disordered phase, (3) insulating ordered phase. The dashed green line denotes the analytical expression (5). (b) A line cut of $\langle m \rangle$ for fixed $\Delta/J = 0.2$ and system size $N = 500$. (c) Finite-size scaling of the magnetization near the critical drive Ω_c. The exponents are $a = 0.55$ and $b = 0.75$ (which agree with $\beta = a/b$). (d) Critical exponent β as a function of γ/J. For $\gamma/J > 0.1$ we extract the critical exponent by fitting the finite-size scaling function [as in (c)], but for weaker dissipation ($\gamma/J \leq 0.1$) we only use the largest available system size due to finite-size effects (see Supplemental Material [34]). Black dashed line represents the analytical prediction $\beta = 1$ in the weak dissipation limit.

The $\hat{A}_s$ matrices are identical to those appearing in previous MPO solutions of incoherently pumped XXZ spin chains [16,22] and are fully determined by the dissipation γ and bulk parameters J and Δ. Unlike those studies, where the right vector $\mathbf{v_R}$ is trivial and determined solely by the boundary dissipation, here it has a more complex structure: it encodes the interplay between the bulk Hamiltonian and the coherent boundary drive. As we show, this nontrivial competition leads to a phase transition with no analog in incoherently pumped models. More generally, the CQA construction employed here allows us to generalize the results of Refs. [16,22], providing a pure steady state of the corresponding doubled system (see Supplemental Material [34]).

Phase diagram—From the exact solution, Eq. (4), we determine the phase diagram of the model, shown in Fig. 2(a) in the Ω, Δ plane. Using the magnetization density $\langle m \rangle \equiv \sum_{i=1}^{N} \mathrm{Tr}(\hat{\sigma}_i^z \hat{\rho}_{\mathrm{ss}})/N$ as an order parameter, we identify three regimes, marked as (1), (2), and (3) in Fig. 2(a). One phase boundary appears along $\Delta/J = 1$, corresponding to a Heisenberg exchange interaction. For $\Delta > J$, the system is always ordered irrespective of Ω. This transition corresponds to the ground-state phase transition of the bulk XXZ spin chain between a Luttinger liquid with ferromagnetic order and a paramagnetic phase [43]. More interesting is the regime $\Delta/J < 1$, where we find an additional, genuinely nonequilibrium transition with no analog in the bulk Hamiltonian.

For $\Delta < J$, we find a continuous transition as Ω is increased from zero, from an ordered state [region (1) with $\langle m \rangle \neq 0$] to a disordered state [region (2) with $\langle m \rangle = 0$] at a critical Ω_c [green dashed line in Fig. 2(a)]. The transition can be understood from a quantum-to-classical mapping of the MPS Eq. (4), under a suitable gauge choice. Local observables, such as the magnetization, can be equivalently calculated from a classical stochastic process consisting of a particle hopping on a chain of N sites. In the weak dissipation limit, $\gamma/J \to 0$ [44], the hopping rates can be analytically obtained and manifest as quasiperiodically disordered rates. Within this classical model, the magnetization corresponds to the average distance traveled in N steps starting from the state $\mathbf{v_L}$ (i.e., site zero), with the final position weighted by the probability distribution corresponding to $\mathbf{v_R}$ (i.e., a postselection). The phase transition can be understood as a localization transition of $\mathbf{v_R}$. In the limit $\gamma/J \to 0$, the coefficient α_k is simply the Chebyshev polynomial of the first kind $\alpha_k(\Omega_c/\Omega) = T_k(\Omega_c/\Omega)$, where [34]

$$\Omega_c = \sqrt{J^2 - \Delta^2}. \tag{5}$$

The phase transition occurs at $\Omega_c/\Omega = 1$ where $\mathbf{v_R}$ transitions from exponentially localized $\alpha_k \sim e^{\xi k}$ with $\cosh \xi = \Omega_c/\Omega$ (for $\Omega < \Omega_c$), which favors trajectories with large excursions away from the initial site (zero), giving rise to $\langle m \rangle \approx -1$, to oscillatory $\alpha_k \sim \cos k\xi$ with $\cos \xi = \Omega_c/\Omega$ (for $\Omega > \Omega_c$), which leads to a disordered state $\langle m \rangle = 0$.

While Eq. (5) is derived from the weak dissipation limit, we numerically find that the critical drive holds approximately for arbitrary dissipation strength [see Fig. 2(b)]. In Supplemental Material [34], we further confirm this by studying the magnetization susceptibility $\partial_\Omega \langle m \rangle$ for different system sizes. Although Ω_c does not directly reflect on the bulk Hamiltonian properties, surprisingly it is proportional to the square root of the smooth part of the infinite-temperature spin Drude weight D [15], which characterizes the ballistic contribution of the real part of the spin conductivity. Further, the Drude weight can be interpreted as an effective velocity squared [45]. Our phase transition thus can be interpreted as a competition between the drive and an effective propagation velocity. This is reminiscent of the phase transition in the asymmetric simple exclusion process (ASEP) [46], which involves an analogous competition between a drive strength and a hopping rate.

Moreover, the phase transition in our model, despite being continuous, does not appear to spontaneously break any symmetries [47], which is another similarity with the ASEP.

To better understand the phase transition, we now turn to the critical behavior near Ω_c, where $|\langle m\rangle| \sim [1-(\Omega/\Omega_c)]^\beta$ for $\Omega < \Omega_c$. We extract the exponent β by a finite-size scaling, shown in Fig. 2(c). Surprisingly, while the critical drive is independent of dissipation, we find that the critical exponent β varies continuously as a function of γ, as shown in Fig. 2(d). In the $\gamma/J \to 0$ limit, we analytically find the exponent $\beta = 1$ (see Supplemental Material [34]), which agrees well with the exponents extracted numerically [Fig. 2(d)].

Another interesting feature in the phase diagram in Fig. 2(a) for $\Delta/J < 1$ is the presence of a set of interaction parameters Δ where the system shows strikingly different behavior. These occur when Δ is tuned to

$$\Delta_{l,m}/J = \cos\frac{l}{m}\pi, \quad m, l \in \mathbb{Z}. \tag{6}$$

For these Δ, and in the weak-γ limit, one can show that the bond dimension of the exact solution MPS in Eq. (4) becomes finite (i.e. independent of system size).

These special points are well known in the fractal structure of the spin Drude weight in the infinite-temperature XXZ model (see, e.g., [13,15,17,48,49]). Here, we find that the magnetization exhibits resonance peaks near each $\Delta_{l,m}$ for $m \lesssim N$ (see Fig. 3), and that there is no phase transition when Δ is exactly tuned to $\Delta_{l,m}$ (see Supplemental Material [34]). The free fermion case is $\Delta_{1,2} = 0$. Our model presents a direct manifestation of this fractal structure in a far more experimentally accessible observable than the Drude weight: the steady-state magnetization. Note that the number of observable resonance peaks is constrained by system size and that their resonance width diminishes with increasing N [see Fig. 3(b)]. This permits the phase transition to persist in the thermodynamic limit for irrational Δ (see Supplemental Material [34]).

Doubled system and hTRS—We now turn to discussing several interesting features of the doubled system of Fig. 1 and consequences of hTRS. To begin, the different phases in Fig. 2 can also be distinguished by the spin current $\langle j\rangle \equiv i\langle(\hat{\sigma}^+_{A,m}\hat{\sigma}^-_{A,m+1} - \text{H.c.})\rangle_{\text{ss}}$. Specifically, phase (3) is insulating, with $\log\langle j\rangle \propto -N$, whereas both phases (1) and (2) are ballistic [the coefficient shows nonanalytic behavior similar to the magnetization in Fig. 2(b) [34]]. Exactly at $\Delta/J = 1$, the current is subdiffusive $\langle j\rangle \sim N^{-2}$, in agreement with previous studies [2,13]. Moreover, the current can also be viewed as the steady-state current of the doubled system in Fig. 1, traveling from the coherent drive on site N of the system, via the chiral waveguide, through the absorber and exiting via the absorber's coherent drive. This implies an exotic situation where the cascaded master equation stabilizes a pure, current-carrying state $|\psi_{\text{CQA}}\rangle$.

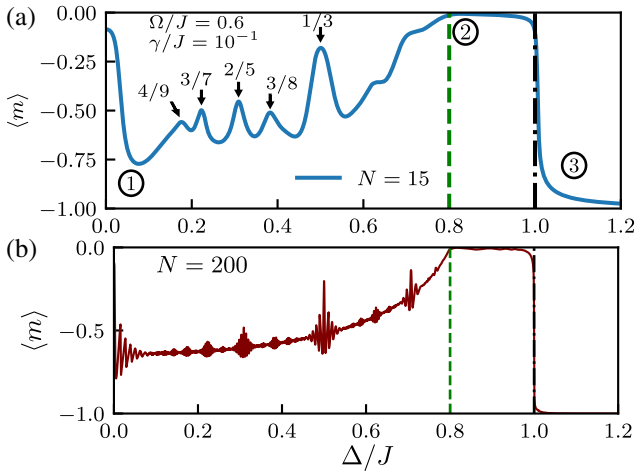

FIG. 3. The steady-state magnetization as a function of Δ/J (a) $N = 15$ and (b) $N = 200$. The green dashed line Eq. (5) and the black dashed line ($\Delta/J = 1$) denotes the phase boundary between phases (1), (2), and (3). In (a) we identify all the resonances due to the special points l/m in Eq. (6). In (b) there are more resonances visible in the larger system.

We stress that there are many ways to experimentally realize such effective chiral waveguides [50].

We also explore quantities unique to the doubled system, with no counterpart in the single spin chain. Using the pure steady state of Eq. (4), we analyze the von Neumann entanglement entropy for a vertical bipartition in Fig. 1: $S_{N/2} = -\text{Tr}(\hat{\rho}_{N/2}\log\hat{\rho}_{N/2})$, where $\hat{\rho}_{N/2} = \text{Tr}_{x>N/2}(|\psi_{\text{CQA}}\rangle\langle\psi_{\text{CQA}}|)$ is the reduced density matrix for half (all sites $x > N/2$) of the combined system absorber. As discussed in the previous section, at the special values of Δ in Eq. (6), the MPS in Eq. (4) has a finite bond dimension, implying area law entanglement, which we confirm numerically in Fig. 4(a). In contrast, away from the special points for $0 < \Delta/J < 1$, we find logarithmic scaling $S_{N/2} \sim \log N$, suggesting linear growth of the bond dimension. Notably, this distinction persists even in the disordered phase (2), where the resonance structures vanish.

Finally, note that the presence of hTRS in our system also constrains its dynamics [23]. In particular, it implies an Onsager symmetry, which takes the form of time-symmetric correlations for certain operators [34],

$$\text{Tr}[\hat{X}(t)\hat{Y}(0)\hat{\rho}_{\text{ss}}] = \text{Tr}[\hat{Y}(t)\hat{X}(0)\hat{\rho}_{\text{ss}}]. \tag{7}$$

Here, $\hat{X}$ and $\hat{Y}$ are the time-symmetric operators predicted by hTRS [34]. In the case of Eq. (1), the following local operators $\hat{X} = \hat{\sigma}^-_1$ and $\hat{Y} = \hat{\sigma}^-_1\hat{\sigma}^-_2$ are time symmetric, which we verified numerically for a small system in Fig. 4(b). In contrast, the spin correlation functions $\langle\hat{\sigma}^z_1(t)\hat{\sigma}^z_2(0)\rangle_{\text{ss}}$ and

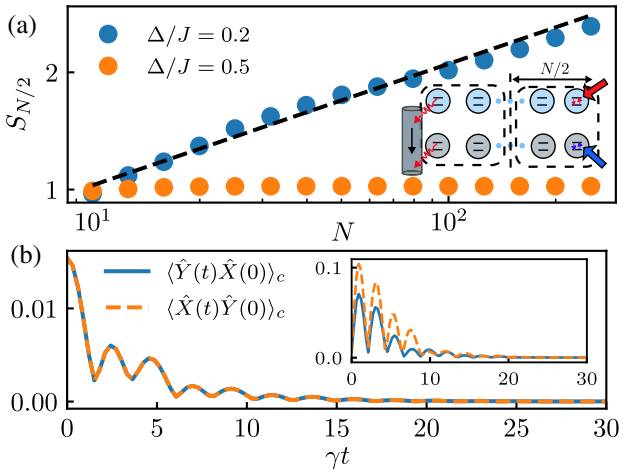

FIG. 4. Features of double construction and hTRS. (a) Entropy scaling for generic anisotropy $\Delta/J = 0.2$ and special point $\Delta/J = \cos(\pi/3) = 0.5$ with $\Omega/J = 2$ and $\gamma/J = 1$. Inset: the bipartition. (b) hTRS: two time correlators for the single chain $N = 3$ where $\hat{X} = \hat{\sigma}_1^-$ and $\hat{Y} = \hat{\sigma}_1^-\hat{\sigma}_2^-$ with $\Omega/J = 0.4$, $\Delta/J = 0.2$, and $\gamma/J = 1$. Inset: $\hat{X} = \hat{\sigma}_1^z$ and $\hat{Y} = \hat{\sigma}_2^z$.

$\langle \hat{\sigma}_2^z(t)\hat{\sigma}_1^z(0)\rangle_{ss}$ are not time symmetric [see Fig. 4(b) inset]. This is related to the fact that the Onsager symmetry does not hold for every pair of operators.

Summary and outlook—In this Letter, we introduced a novel exact solution to the boundary coherent-driven-dissipative XXZ spin chain with an explicit doubled state construction. This allowed us to identify a unique continuous dissipative phase transition as a function of the boundary drive amplitude. We also found that simple observables in the dissipative steady state directly manifest fractal behavior controlled by anisotropy Δ/J. Our Letter suggests that coherently driven-dissipative models could be a rich source of new phenomena and insights. While our Letter focuses on the phase transition in the thermodynamic limit, intriguing phenomena exist for small system sizes, such as the fractal resonance structure and subtle hTRS symmetry; these are extremely well suited for near-term quantum simulation experiments.

Acknowledgments—We acknowledge helpful discussions with R. Vasseur, M. Maghrebi, T. Jin, and S. Gopalakrishnan. This work was supported by the Army Research Office under Grant No. W911NF-23-1-0077, the National Science Foundation QLCI HQAN (NSF Grant No. 2016136), the Air Force Office of Scientific Research MURI program under Grant No. FA9550-19-1-0399, and the Simons Foundation through a Simons Investigator Award (Grant No. 669487), and partially supported by the University of Chicago Materials Research Science and Engineering Center, which is funded by the National Science Foundation under Grant No. DMR-2011854.

[1] B. Bertini, F. Heidrich-Meisner, C. Karrasch, T. Prosen, R. Steinigeweg, and M. Žnidarič, Rev. Mod. Phys. **93**, 025003 (2021).
[2] G. T. Landi, D. Poletti, and G. Schaller, Rev. Mod. Phys. **94**, 045006 (2022).
[3] E. Ilievski, J. De Nardis, S. Gopalakrishnan, R. Vasseur, and B. Ware, Phys. Rev. X **11**, 031023 (2021).
[4] X. Mi, A. A. Michailidis, S. Shabani, K. C. Miao, P. V. Klimov, J. Lloyd, E. Rosenberg, R. Acharya, I. Aleiner, T. I. Andersen, M. Ansmann, F. Arute, K. Arya *et al.*, Science **383**, 1332 (2024).
[5] D. Wei, A. Rubio-Abadal, B. Ye, F. Machado, J. Kemp, K. Srakaew, S. Hollerith, J. Rui, S. Gopalakrishnan, N. Y. Yao, I. Bloch, and J. Zeiher, Science **376**, 716 (2022).
[6] E. Rosenberg, T. I. Andersen, R. Samajdar, A. Petukhov, J. C. Hoke, D. Abanin, A. Bengtsson, I. K. Drozdov, C. Erickson, P. V. Klimov, X. Mi, A. Morvan, M. Neeley, C. Neill, R. Acharya, R. Allen, K. Anderson, M. Ansmann *et al.*, Science **384**, 48 (2024).
[7] M. Boll, T. A. Hilker, G. Salomon, A. Omran, J. Nespolo, L. Pollet, I. Bloch, and C. Gross, Science **353**, 1257 (2016).
[8] S. Scherg, T. Kohlert, J. Herbrych, J. Stolpp, P. Bordia, U. Schneider, F. Heidrich-Meisner, I. Bloch, and M. Aidelsburger, Phys. Rev. Lett. **121**, 130402 (2018).
[9] M. Ljubotina, M. Žnidarič, and T. Prosen, Nat. Commun. **8**, 16117 (2017).
[10] E. Ilievski, J. De Nardis, M. Medenjak, and T. Prosen, Phys. Rev. Lett. **121**, 230602 (2018).
[11] B. Ye, F. Machado, J. Kemp, R. B. Hutson, and N. Y. Yao, Phys. Rev. Lett. **129**, 230602 (2022).
[12] M. Ljubotina, M. Žnidarič, and T. Prosen, Phys. Rev. Lett. **122**, 210602 (2019).
[13] T. Prosen, Phys. Rev. Lett. **106**, 217206 (2011).
[14] M. Znidarič, Phys. Rev. Lett. **106**, 220601 (2011).
[15] T. Prosen and E. Ilievski, Phys. Rev. Lett. **111**, 057203 (2013).
[16] T. Prosen, Phys. Rev. Lett. **107**, 137201 (2011).
[17] E. Ilievski and J. De Nardis, Phys. Rev. Lett. **119**, 020602 (2017).
[18] T. Prosen, E. Ilievski, and V. Popkov, New J. Phys. **15**, 073051 (2013).
[19] T. Prosen, Phys. Rev. Lett. **112**, 030603 (2014).
[20] T. Prosen, J. Phys. A **48**, 373001 (2015).
[21] T. Prosen and I. Pizorn, Phys. Rev. Lett. **101**, 105701 (2008).
[22] D. Karevski, V. Popkov, and G. M. Schütz, Phys. Rev. Lett. **110**, 047201 (2013).
[23] D. Roberts, A. Lingenfelter, and A. A. Clerk, PRX Quantum **2**, 020336 (2021).
[24] K. Stannigel, P. Rabl, and P. Zoller, New J. Phys. **14**, 063014 (2012).
[25] D. Roberts and A. A. Clerk, Phys. Rev. Lett. **130**, 063601 (2023).
[26] D. Roberts and A. A. Clerk, Phys. Rev. Lett. **131**, 190403 (2023).
[27] D. Roberts and A. A. Clerk, Phys. Rev. X **10**, 021022 (2020).
[28] A. Lingenfelter, M. Yao, A. Pocklington, Y.-X. Wang, A. Irfan, W. Pfaff, and A. A. Clerk, Phys. Rev. X **14**, 021028 (2024).

[29] M. Fitzpatrick, N. M. Sundaresan, A. C. Y. Li, J. Koch, and A. A. Houck, Phys. Rev. X **7**, 011016 (2017).
[30] A. Prem, V. B. Bulchandani, and S. L. Sondhi, Phys. Rev. B **107**, 104304 (2023).
[31] G. P. Fedorov, S. V. Remizov, D. S. Shapiro, W. V. Pogosov, E. Egorova, I. Tsitsilin, M. Andronik, A. A. Dobronosova, I. A. Rodionov, O. V. Astafiev, and A. V. Ustinov, Phys. Rev. Lett. **126**, 180503 (2021).
[32] M. Kounalakis, C. Dickel, A. Bruno, N. K. Langford, and G. A. Steele, npj Quantum Inf. **4**, 38 (2018).
[33] P. Scholl, H. J. Williams, G. Bornet, F. Wallner, D. Barredo, L. Henriet, A. Signoles, C. Hainaut, T. Franz, S. Geier, A. Tebben, A. Salzinger, G. Zürn, T. Lahaye, M. Weidemüller, and A. Browaeys, PRX Quantum **3**, 020303 (2022).
[34] See Supplemental Material at http://link.aps.org/supplemental/10.1103/PhysRevLett.134.130404 for additional discussion on the definition of the exact solution, proof of uniqueness, and phenomenology derived from the exact solution, which includes Refs. [1,16,19,20,22–24,28,35–39].
[35] B. Kraus, H. P. Büchler, S. Diehl, A. Kantian, A. Micheli, and P. Zoller, Phys. Rev. A **78**, 042307 (2008).
[36] Y. Zhang and T. Barthel, J. Phys. A **57**, 115301 (2024).
[37] A. Frigerio, Lett. Math. Phys. **2**, 79 (1977).
[38] Y. G. Sinai, Theory Probab. Appl. **27**, 256 (1983).
[39] U. Agrawal, S. Gopalakrishnan, R. Vasseur, and B. Ware, Phys. Rev. B **101**, 224415 (2020).
[40] H. J. Carmichael, Phys. Rev. Lett. **70**, 2273 (1993).
[41] C. W. Gardiner, Phys. Rev. Lett. **70**, 2269 (1993).
[42] A. Metelmann and A. A. Clerk, Phys. Rev. A **95**, 013837 (2017).
[43] F. Franchini, *An Introduction to Integrable Techniques for One-Dimensional Quantum Systems* (Springer, New York, 2017).
[44] As in many driven-dissipative systems, the order of taking the weak dissipation limit $\gamma/J \to 0$ and the thermodynamic limit $N \to \infty$ do not commute. Here we first take the thermodynamic limit, then investigate the system with vanishing dissipation.
[45] J. D. Nardis, D. Bernard, and B. Doyon, SciPost Phys. **6**, 049 (2019).
[46] B. Derrida, Phys. Rep. **301**, 65 (1998).
[47] F. Minganti, I. Arkhipov, A. Miranowicz, and F. Nori, New J. Phys. **23**, 122001 (2021).
[48] U. Agrawal, S. Gopalakrishnan, R. Vasseur, and B. Ware, Phys. Rev. B **101**, 224415 (2020).
[49] V. B. Bulchandani, S. Gopalakrishnan, and E. Ilievski, J. Stat. Mech. (2021) 084001.
[50] X. Cao, A. Irfan, M. Mollenhauer, K. Singirikonda, and W. Pfaff, Phys. Rev. Applied **22**, 064023 (2024).